Prediction of the structural and electronic properties of MoxTi1xS2 monolayers via first principle simulations

NANOMATERIALS AND NANOTECHNOLOGY

Nanomaterials and Nanotechnology
Volume 10: 1–6

DOI: 10.1177/1847980420955093
journals.sagepub.com/home/nax
SAGE

Prediction of the structural and electronic properties of $Mo_xTi_{1-x}S_2$ monolayers via first principle simulations

Ankit Kumar Verma[1], Federico Raffone[2], and Giancarlo Cicero[1]

Abstract

Two-dimensional transition metal dichalcogenides have gained great attention because of their peculiar physical properties that make them interesting for a wide range of applications. Lately, alloying between different transition metal dichalcogenides has been proposed as an approach to control two-dimensional phase stability and to obtain compounds with tailored characteristics. In this theoretical study, we predict the phase diagram and the electronic properties of $Mo_xTi_{1-x}S_2$ at varying stoichiometry and show how the material is metallic, when titanium is the predominant species, while it behaves as a *p*-doped semiconductor, when approaching pure MoS_2 composition. Correspondingly, the thermodynamically most stable phase switches from the tetragonal to the hexagonal one. Further, we present an example which shows how the proposed alloys can be used to obtain new vertical two-dimensional heterostructures achieving effective electron/hole separation.

Keywords

2D materials, alloys, formation energy, ALD

Date received: 30 April 2020; accepted: 30 July 2020

Topic: Low Dimensional Semiconductor and Graphene-like Nanostructures
Topic Editor: Rajesh Kappera
Associate Editor: Fabrizio Cleri

Introduction

The discovery of single-layer graphene[1] opened up the opportunity to realize innovative devices with outstanding performances such as field effects transistors (FETs) with unprecedented sensitivity. However, because of the lack of a bandgap, the applicability of graphene is limited. Recent research was devoted to find suitable two-dimensional (2D) alternatives such as hexagonal boron nitride,[2] black phosphorus,[3] graphene oxide,[4] silicene,[5] and transition metal dichalcogenides (TMDs).[6]

TMDs are probably the most studied 2D compounds because of their tunable properties, which depend on their specific constituent elements and on their structure. The typical TMDs formula unit is MX_2, where M represents a transition metal, while X corresponds to a chalcogen atom. Different M and X combinations offer a large pool of materials with wide range of properties which make them interesting building blocks for the realization of innovative sensors,[7] FETs,[8] solar cells,[9] light emitting diodes (LEDs),[10] and so on. Further, a given TMD can be usually found in distinct phases (polytypes) differing for the geometry of the metal coordination: a trigonal prismatic coordination (H-phase) and an octahedral one (T-phase).[11] Some TMDs are thermodynamically more stable in the

[1] Department of Applied Science and Technology, Politecnico di Torino, Torino, Italy
[2] Department of Chemistry, Imperial College London, London, UK

Corresponding author:
Federico Raffone, Department of Chemistry, Imperial College London, White City Campus, 80 Wood Lane, London W12 0BZ, UK.
Email: f.raffone@imperial.ac.uk

H-phase while others are more stable in the T one; few compounds, such as MoS_2, also exist in a distorted T-phase often referred as ZT or T′-phase.[11,12] Typically, changing the metal coordination modifies the hybridization of the d orbital involved in bonding with the chalcogen atoms and, consequently, it may alter the bandgap of the system[6] which, in many cases, passes from being metallic to semiconducting or vice versa. Different methods have been proposed to revert the phase stability of TMDs and, thus, control their electronic properties. For example, Rajesh Kappera et al.[13] have shown that lithium intercalation in multilayer MoS_2 induces a permanent phase change from the stable semiconducting phase to the metastable metallic one leading to a decrease of the contact resistance in the devices. Reversible phase switching has also been achieved by hot electron injection into the 2D layer from plasmonic metal nanoparticles deposited on MoS_2.[14] Another promising strategy, currently employed to engineer TMD monolayers, consists of alloying two different TMD compounds.[15–17] Typically, it is either possible to substitute part of the metal atoms of a given MX_2 with a different metal species (M′) which also exist in the form of a 2D structure ($M'X_2$) to obtain $M_xM'_{1-x}X_2$ alloys or it is possible to replace X with a different chalcogen atom (X′) to obtain $MX_xX'_{2-x}$. In limited cases, the possibility to vary both the metal and the chalcogen species has been explored.[18] For example, Pandey et al. have studied ordered mixtures of various TMDs[19] demonstrating the impact of alloying on the properties of the outcoming material, but in their study they restricted only to specific compositions. In another recent work, Raffone et al.[20] proved that combining density functional theory (DFT) simulations and cluster expansion (CE) calculations represent an effective way to predict the structural and electronic properties of TMD alloys in their full compositional range, and, in particular, they showed how a small addition of a substitutional metal atom is able to change the relative phase stability in MoS_2.

In this article, we aim at studying the phase diagram and physical properties of novel alloys obtained by combining MoS_2 and TiS_2 employing the computational strategy presented by Raffone et al.[20] We have chosen to focus on MoS_2 because several experimental studies proved that atomic layer deposition can be applied to growth monolayer MoS_2 on conventional substrates,[21] followed by the deposition of another 2D materials to fabricate vertical heterostructures;[22] these may then be used in devices such as solar cells, LEDs, FETs, photodiodes, and sensors. TiS_2 was instead chosen because it is characterized by a very small lattice mismatch with MoS_2, thus this couple may originate alloys characterized by reduced strain and good thermodynamic stability. Moreover, since titanium (Ti) atoms have two d valence electrons less than MoS_2, similar to niobium impurities,[23] it may originate *p*-type character structures and modify the intrinsic *n*-type character of MoS_2. This would open up the way for the realization of sharp bilayer heterojunctions achieving efficient electron–hole separation, as proved by the example presented in the last part of the article.

Methods

The prediction of the structure, stability, and electronic properties of MoS_2, TiS_2, and their alloys has been carried out by combining DFT and CE. The CE simulations were performed by employing the ATAT, version 3.04[24] software, while for the DFT calculations we used the plane-wave approach as coded in the QUANTUM ESPRESSO, version 6.0[25] software package. The coupled CE-DFT approach is a well-established method that allows predicting with great accuracy alloy phase diagrams in their full composition range.[26] In particular, the phase diagram construction proceeds by following a step-by-step process involving alternating DFT simulations and CE predictions. The software implementing CE proposes an appropriate alloy structure as input to the DFT code and, at the end of the quantum simulation, the total energy is returned to the CE program. The DFT total energies are the basic elements used to obtain interaction coefficients among groups of atoms in the alloy, also referred as effective cluster interactions, which then determine the configurational energy of any structure at varying concentrations such that the most stable one is identified. In this way, the expansion is used to predict the energy of all configurations for the full concentration range, accessing also those arrangements that are computationally too demanding for DFT and preventing the need for an extremely large set of ab initio simulations.[27] This approach has been successfully applied to the prediction of other 2D TMD alloys.[20] Concerning the DFT methodology, the Perdew–Burke–Ernzerhof functional[28] was employed to account for exchange–correlation energy and the electron–ion interaction was described by ultrasoft pseudopotentials. A plane-wave energy cutoff of 50 Ry (500 Ry) for the wave functions (electron densities). The k-point grid was set to ($8 \times 8 \times 1$) for MoS_2 and TiS_2 monolayer primitive cells and reduced accordingly for supercell calculations, so to keep constant the density of the k-point mesh in the reciprocal space. A vacuum region of about 10 Å was introduced in the supercell in the direction perpendicular to the monolayer to avoid spurious interactions between periodic replicas; structure relaxation was assumed at convergence when the maximum component of the residual forces on the ions was smaller than 10^{-5} Ry/Bohr. In the case of the heterojunction, the minimum energy structure was obtained by applying the DFT-D2 correction to account for dispersive interactions between layers.[29] For each $Mo_xTi_{1-x}S_2$ alloy configuration, the formation energy, both for DFT and CE simulations, was calculated as follows

$$E_{\text{form}} = E_{\text{Mo}_x\text{Ti}_{1-x}\text{S}_2} - [xE_{\text{H-MoS}_2} + (1-x)E_{\text{TiS}_2}]$$

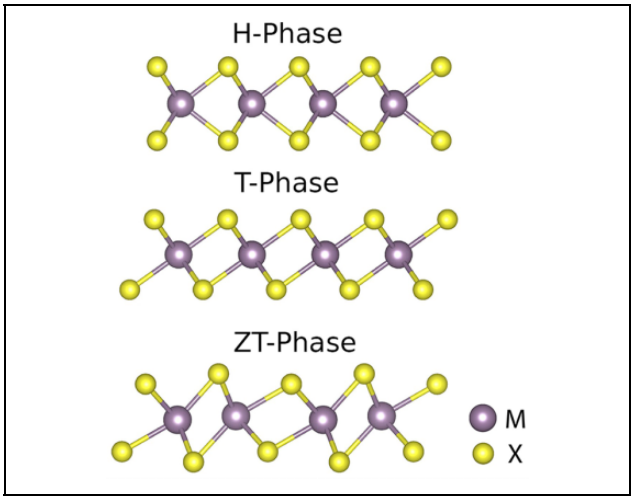

Figure 1. Balls and sticks representations of the three typical 2D-TMDs polytypes (H, T, and ZT phases). Yellow and violet spheres represent the chalcogen and metal atoms, respectively. TMD: transition metal dichalcogenide.

Table 1. *a* and *b*, E_g, and ΔE between the most stable phase (taken as zero of energy) and the least stable one for both TiS_2 and MoS_2 monolayers.

TMDs	*a* (Å)	*b* (Å)	E_g (eV)	ΔE (eV/cell)
H-TiS_2	3.34	3.34	0.73	0.43
T-TiS_2	3.41	3.41	0.05	0.00
H-MoS_2	3.19	3.19	1.58	0.00
ZT-MoS_2	3.18	5.74	0.06	0.55

a and *b*: equilibrium lattice parameters; E_g: bandgap energy; ΔE: total energy difference per primitive cell; TMD: transition metal dichalcogenide.

where $E_{Mo_xTi_{1-x}S_2}$, E_{H-MoS_2}, and E_{TiS_2} are respectively the total energies of the alloy, of the H-MoS_2 and T-TiS_2 monolayers, while x is the Mo concentration.

Results and discussion

As introduced earlier, MoS_2 and TiS_2 monolayers exist in different polytype structures, thus, before discussing their alloys, we here revise the relative stability, the structural and electronic properties of their pure phases as found at DFT level. In particular, MoS_2 presets a stable H-phase which is semiconducting and a distorted metastable T-phase, usually called ZT or T′, which has a very small bandgap (see structures in Figure 1). The undistorted T-phase would be metallic, but it is unstable and spontaneously relaxes to ZT. For TiS_2 on the contrary the most stable phase is T, which is reported to be metallic[30] or with a very small bandgap, the H-phase is metastable while the distorted ZT does not exist. The results of our simulations, summarized in Table 1, are in agreement with previously reported data[20,30,31] and confirm the picture described above. H-MoS_2 has a bandgap of 1.58 eV which reduces to 0.06 eV in the ZT-phase in exact agreement with what

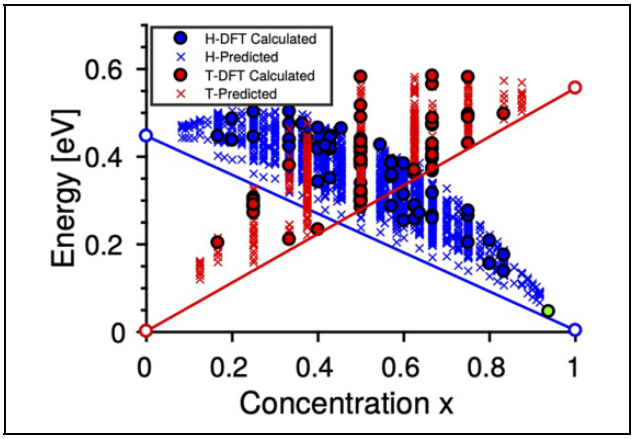

Figure 2. $Mo_xTi_{1-x}S_2$ phase diagram showing the DFT calculated formation energies for the H (encircled blue dots) and T (encircled red dots) phases and the resulting predicted energies obtained from CE for the H (blue cross marks) and T (red cross marks) phases. The encircled green dot represents the DFT formation energy of a specific alloy composition $Mo_{0.9375}Ti_{0.0625}S_2$ with H structure. DFT: density functional theory; CE: cluster expansion.

reported by Raffone et al.[20] In the case of Ti, T-TiS_2 has a very small bandgap of 0.05 eV (unlike Xu et al.,[30] bands do not overlap), while for the H-phase the energy gap amounts to 0.73 eV. An analysis of the predicted equilibrium lattice parameters (see Table 1) reveals that the stable phases of the two compounds (H-MoS_2 and T-TiS_2) are characterized by a small lattice mismatch (about 6%). It could be, then, possible to obtain a stable alloy from these materials. Moreover the different electronic properties of the two compounds in their stable structure open up the possibility to tune the bandgap and other electronic properties in a wide range of values through alloying.

To obtain the phase diagram of $Mo_xTi_{1-x}S_2$, we computed separately the CE of the alloy in the H and ZT/T phases in the full range of x variability. The results of the formation energies as a function of the alloy composition are summarized in Figure 2, where the two reference energies are T-TiS_2 total energy for $x = 0$ and H-MoS_2 total energy for $x = 1$. The graph shows how the formation energy of the alloys in a given structure (H or T) varies with respect to these reference energies. In particular, the red and blue encircled dots (cross marks) represent the alloy energy calculated by means of DFT (CE) simulations for the H-phase and T-phase respectively. The values represented with crosses correspond to the CE configuration energies as obtained on the basis of the DFT results. Further, the solid lines in the plot represent the minimum energy structures throughout the whole x range and originate the so-called convex hull shape. The phase diagram clearly proves that as the concentration of Ti increases in MoS_2 (x values close to 1 or smaller) the alloy formation energies increase for the H-phase but they decrease for the T-phase. On the contrary, as more Ti atoms in TiS_2 are

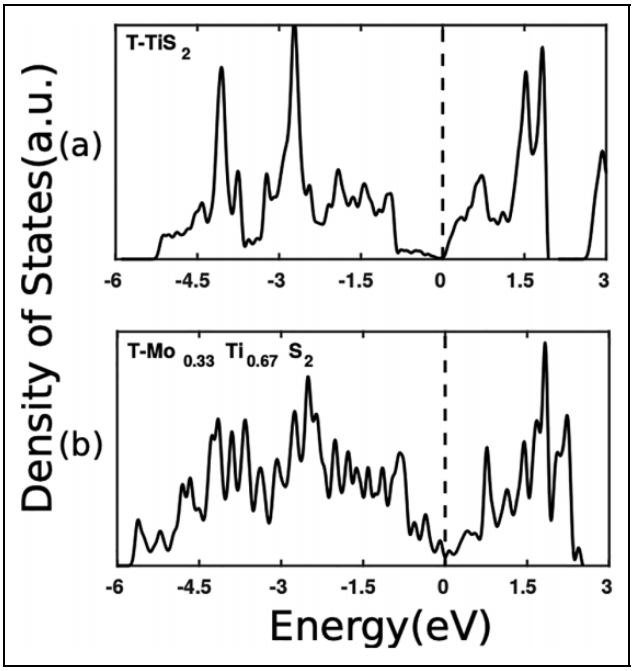

Figure 3. Density of states of (a) TiS2 and (b) $Mo_{0.33}Ti_{0.67}S_2$ in their lowest energy T structure. Dashed line corresponds to the Fermi level, taken as zero of energy.

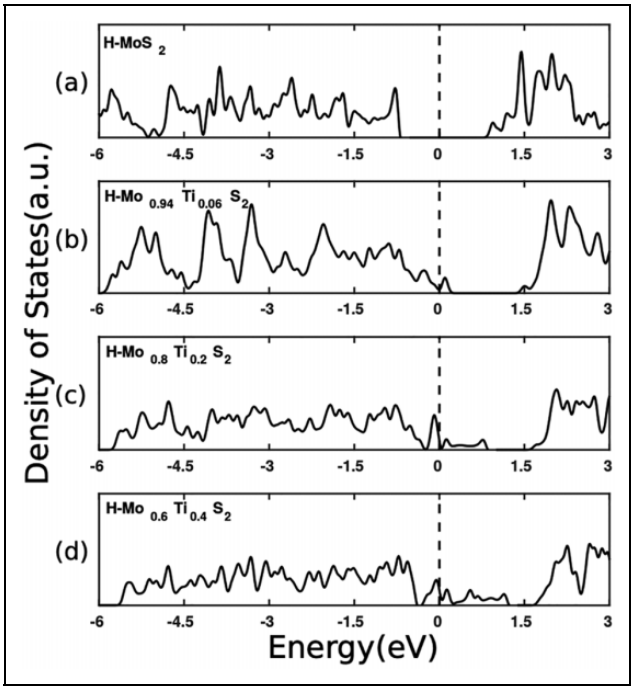

Figure 4. Density of states of (a) MoS_2, (b) H-$Mo_{0.9375}Ti_{0.0625}S_2$, (c) H-$Mo_{0.8}Ti_{0.2}S_2$, and (d) H-$Mo_{0.6}Ti_{0.4}S_2$ in their lowest energy H-structure. Dashed line corresponds to the Fermi level, taken as zero of energy.

substituted with Mo atoms (x values close to zero or larger); the alloy formation energies increase for the T-phase but they decrease for the H-phase. It is apparent that a cross-over between the two phases occurs at Mo concentration $x = 0.45$. Below this point the alloy is more stable in the T-phase: The Ti atoms are the majority metal species and thus the more stable structure of TiS_2 is retained; for xx larger than 0.45, the H-phase becomes more stable as the Mo metal species becomes predominant. A similar behavior has been observed for $Mo_xSn_{1-x}S_2$ alloys in a previously published work.[20]

We now discuss, how the electronic properties of the lowest energy alloy structures change as a function of the composition. To this aim, we analyzed the density of states (DOS) and the bandgap of $Mo_xTi_{1-x}S_2$ along the convex hull line. All the compounds with x smaller than 0.45, retaining T structure typical of TiS_2, appear to be metallic: None of them present an energy gap between the valence and conduction band. As an example representative of this stoichiometry range, we reported in Figure 3 the comparison between the DOS of the pure T-TiS_2 and that of $Mo_{0.33}Ti_{0.67}S_2$. It is apparent that the presence of Mo atoms in TiS_2 increases the number of states at the Fermi level, which would correspond to an increase of the conductivity in the alloyed compounds with respect to pure TiS_2.

The electronic features of $Mo_xTi_{1-x}S_2$ samples with $x > 0.45$ are summarized in Figure 4, where we show the DOS of four representative samples with an increasing amount of Ti atoms. It is evident that in the DOS of the sample with low Ti concentration (e.g. green circle of Figure 2) acceptor states appear right above the top of the valence band of the system if compared to the DOS of pure H-MoS_2. Namely, Ti atoms, when substituting molybdenum, act as p-type dopants for H-MoS_2, consistently with the fact that they have two less valence electrons in comparison to Mo. As the concentration of Ti increases, the number of acceptor states above the Fermi level increases; correspondingly their spread in energy is wider and the effective energy gap between the highest energy acceptor states and the conduction band minimum decreases, as clearly evident from Figure 4(a) to (d).

Having found that $Mo_xTi_{1-x}S_2$ alloys with small amount of Ti are characterized by p polarity, we further investigated if these structures can be employed in 2D vertical heterostructures to effectively achieve electron–hole separation between the two layers. To this aim, we interfaced a low - energy p-type monolayer, such as the one represented by the encircled green dot in Figure 2, with an n-type structure. Recently, it has been shown that an effective way to obtain n-doped H-MoS_2 consists of surface functionalization with organic moieties such as alkyl groups[32] or $-$H fragments;[33] these fragments generate shallow donor states and move the Fermi level of H-MoS_2 close to the bottom of its conduction band. We thus built a bilayer system obtained by stacking H-$Mo_{0.9375}Ti_{0.0625}S_2$ with H-MoS_2 which adsorbed a $-CH_3$ fragment and a hydrogen atom on its surface (see the structure reported in Figure 5).

An analysis of the DOS projected on the n- and p-type monolayers reported in Figure 6 reveals that, when the

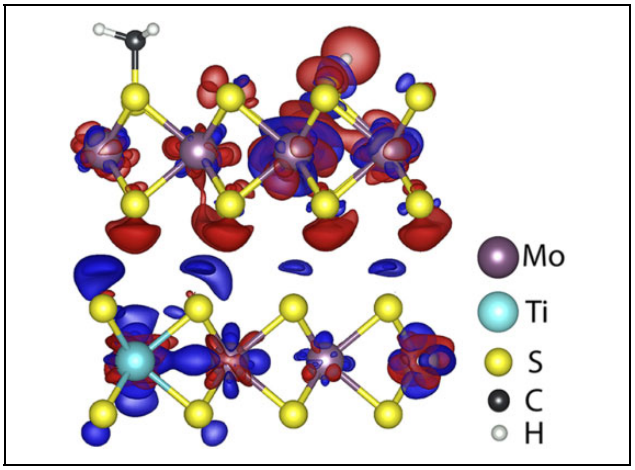

Figure 5. Balls and sticks representation of the heterostructure obtained by stacking H-$Mo_{0.9375}Ti_{0.0625}S_2$ (bottom layer) and an H-MoS_2 which adsorbed a $-CH_3$ fragment and a hydrogen atom (top layer). Yellow, violet, and cyan spheres represent S, Mo, and Ti atoms respectively. White and black spheres correspond to hydrogen and carbon species respectively. The blue (red) isosurface corresponds to electron charge accumulation (depletion) with respect to the isolated monolayers.

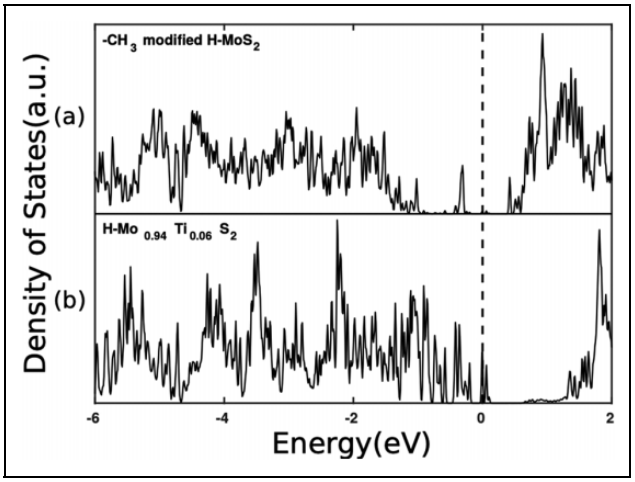

Figure 6. Density of states projected on the (a) functionalized H-MoS_2 layer and on the (b) H-$Mo_{0.9375}Ti_{0.0625}S_2$ layer of the heterostructure. Dashed line corresponds to the Fermi level, taken as zero of energy.

junction is formed, the donor states of the $-CH_3$ modified H-MoS_2 layer are partially emptied and the electrons are transferred to the acceptors states of the H-$Mo_{0.9375}Ti_{0.0625}S_2$, which become partially filled. Due to this partial filling, the Fermi level of the heterostructure raises if compared to the DOS of isolated H-$Mo_{0.9375}Ti_{0.0625}S_2$ (see to the DOS reported in panel (b) of Figure 4). To highlight the charge transfer occurring at the heterojunction, we calculated the electron density difference between the interacting bilayer systems and isolated ones: The blue isosurface of Figure 5 represents charge accumulation, while the red isosurface represents charge depletion. It is apparent that most of the blue isosurface is localized in the bottom layer (*p*-type H-$Mo_{0.9375}Ti_{0.0625}S_2$), while the largest part of the red isosurface is localized in the upper layer (*n*-type organic functionalized H-MoS_2). Consistently with the picture gained by the PDOS analysis, a spontaneous charge transfer from the *n*- to the *p*-type layer of the heterostructure occurs that originates an effective electron–hole separation between the two layers. The entity of transferred charge has been qualitatively confirmed by calculating the sum of the Löwdin charges of each layer before and after the formation of the junction and amounts to 0.13 electrons/cell.

Conclusions

In summary, in this article, we have predicted the thermodynamic stability and the electronic properties of $Mo_xTi_{1-x}S_2$ monolayers in the full range of x variability. We have found that the alloys exist in the T-phase structure, typical of pure TiS_2 monolayer, when the concentration of Mo, x, is smaller than 0.45, and that in this regime the monolayer has metallic character. On the contrary for x values larger than 0.45, the monolayer is more stable in the H-phase, the samples are semiconducting and show *p*-type polarity. With this respect, alloying H-MoS_2 and T-TiS_2 appears to be an effective approach to engineer the physical properties of these 2D structures. Lastly, we have proposed an example of application of our studied systems by realizing a vertical heterostructure composed of $Mo_xTi_{1-x}S_2$ (at low Ti concentration) and $-CH_3$ functionalized H-MoS_2. In this system, due to the *p*–*n* character of the junctions, electron/hole spatial separation between the two layers is achieved. We propose that such type of heterostructures could be employed in innovative nanostructured devices such as solar cells or sensors.

Acknowledgments

The authors acknowledge the CINECA award under the ISCRA initiative and HPC@POLITO, for the availability of high-performance computing resources and support.

Declaration of conflicting interests

The author(s) declared no potential conflicts of interest with respect to the research, authorship, and/or publication of this article.

Funding

The author(s) received no financial support for the research, authorship, and/or publication of this article.

ORCID iD

Federico Raffone https://orcid.org/0000-0001-5045-7533

References

1. Novoselov KS, Geim AK, Morozov SV, et al. Electric field effect in atomically thin carbon films. *Science* 2004; 306(5696): 666–669.

2. Grüning M and Attaccalite C. Second harmonic generation in *h*-BN and MoS_2 monolayers: role of electron–hole interaction. *Phys Rev B* 2014; 89(8): 081102.
3. Rodin A, Carvalho A, and Neto AC. Strain-induced gap modification in black phosphorus. *Phys Rev Lett* 2014; 112(17): 176801.
4. Savazzi F, Risplendi F, Mallia G, et al. Unravelling some of the structure–property relationships in graphene oxide at low degree of oxidation. *J Phys Chem Lett* 2018; 9: 1746–1749.
5. Oughaddou H, Enriquez H, Tchalala MR, et al. Silicene, a promising new 2D material. *Prog Surf Sci* 2015; 90(1): 46–83.
6. Chhowalla M, Shin HS, Eda G, et al. The chemistry of two-dimensional layered transition metal dichalcogenide nanosheets. *Nat Chem* 2013; 5(4): 263–275.
7. Ping J, Fan Z, Sindoro M, et al. Recent advances in sensing applications of two-dimensional transition metal dichalcogenide nanosheets and their composites. *Adv Funct Mater* 2017; 27(19): 1605817.
8. Rawat B, Vinaya M, and Paily R. Transition metal dichalcogenide-based field-effect transistors for analog/mixed-signal applications. *IEEE Trans Electron Devices* 2019; 66(5): 2424–2430.
9. Tsai ML, Su SH, Chang JK, et al. Monolayer MoS_2 heterojunction solar cells. *ACS Nano* 2014; 8(8): 8317–8322.
10. Yang W, Shang J, Wang J, et al. Electrically tunable valley-light emitting diode (vLED) based on CVD-grown monolayer WS_2. *Nano Lett* 2016; 16(3): 1560–1567.
11. Ataca C, Sahin H, and Ciraci S. Stable, single-layer MX_2 transition-metal oxides and dichalcogenides in a honeycomb-like structure. *J Phys Chem C* 2012; 116(16): 8983–8999.
12. Kan M, Wang JY, Li XW, et al. Structures and phase transition of a MoS_2 monolayer. *J Phys Chem C* 2014; 118(3): 1515–1522.
13. Kappera R, Voiry D, Yalcin SE, et al. Phase-engineered low-resistance contacts for ultrathin MoS_2 transistors. *Nat Mater* 2014; 13(12): 1128–1134.
14. Kang Y, Najmaei S, Liu Z, et al. Plasmonic hot electron induced structural phase transition in a MoS_2 monolayer. *Adv Mater* 2014; 26(37): 6467–6471.
15. Kang J, Tongay S, Li J, et al. Monolayer semiconducting transition metal dichalcogenide alloys: stability and band bowing. *J Appl Phys* 2013; 113(14): 143703.
16. Komsa HP and Krasheninnikov AV. Two-dimensional transition metal dichalcogenide alloys: stability and electronic properties. *J Phys Chem Lett* 2012; 3(23): 3652–3656.
17. Gusakova J, Gusakov V, and Tay BK. DFT study of structural and electronic properties of $MoS_2(1-x)Se_2x$ alloy ($x = 0.25$). *J Appl Phys* 2018; 123(16): 161594.
18. Susarla S, Kutana A, Hachtel JA, et al. Quaternary 2D transition metal dichalcogenides (TMDs) with tunable bandgap. *Adv Mater* 2017; 29(35): 1702457.
19. Pandey M, Jacobsen KW, and Thygesen KS. Atomically thin ordered alloys of transition metal dichalcogenides: stability and band structures. *J Phys Chem C* 2016; 120(40): 23024–23029.
20. Raffone F, Ataca C, Grossman JC, et al. MoS_2 enhanced T-phase stabilization and tunability through alloying. *J Phys Chem Lett* 2016; 7(13): 2304–2309.
21. Tan LK, Liu B, Teng JH, et al. Atomic layer deposition of a MoS_2 film. *Nanoscale* 2014; 6(18): 10584–10588.
22. Kim HG and Lee HBR. Atomic layer deposition on 2D materials. *Chem Mater* 2017; 29(9): 3809–3826.
23. Das S, Demarteau M, and Roelofs A. Nb-doped single crystalline MoS_2 field effect transistor. *Appl Phys Lett* 2015; 106(17): 173506.
24. van de Walle A. Multicomponent multisublattice alloys, nonconfigurational entropy and other additions to the Alloy Theoretic Automated Toolkit. *Calphad* 2009; 33: 266–278.
25. Giannozzi P, Baroni S, Bonini N, et al. QUANTUM ESPRESSO: a modular and open-source software project for quantum simulations of materials. *J Phys Condens Matter* 2009; 21(39): 395502 (19pp).
26. Seko A, Koyama Y, and Tanaka I. Cluster expansion method for multicomponent systems based on optimal selection of structures for density-functional theory calculations. *Phys Rev B* 2009; 80(16): 165122.
27. van de Walle A and Ceder G. Automating first-principles phase diagram calculations. *J Phase Equilib* 2002; 23(4): 348.
28. Perdew JP, Burke K, and Ernzerhof M. Generalized gradient approximation made simple. *Phys Rev Lett* 1996; 77(18): 3865–3868.
29. Grimme S. Semiempirical GGA-type density functional constructed with a long-range dispersion correction. *J Comput Chem* 2006; 27(15): 1787–1799.
30. Xu C, Brown PA, and Shuford KL. Strain-induced semimetal-to-semiconductor transition and indirect-to-direct band gap transition in monolayer 1T-TiS_2. *RSC Adv* 2015; 5(102): 83876–83879.
31. Postorino S, Grassano D, D'Alessandro M, et al. Strain-induced effects on the electronic properties of 2D materials. *Nanomater Nanotechnol* 2020; 10. https://journals.sagepub.com/doi/full/10.1177/1847980420902569.
32. Palummo M, D′Auria AN, Grossman JC, et al. Tailoring the optical properties of MoS_2 and WS_2 single layers via organic functionalization. *J Phys Condens Matter* 2019; 31: 235701.
33. Singh A and Singh AK. Origin of *n*-type conductivity of monolayer MoS_2. *Phys Rev B* 2019; 99(12): 121201.